



Nutations in Plant Shoots: Endogenous and Exogenous Factors in the Presence of Mechanical Deformations

Daniele Agostinelli^{1*†}, Antonio DeSimone^{1,2} and Giovanni Noselli¹

¹ SISSA–International School for Advanced Studies, Trieste, Italy, ² The BioRobotics Institute, Scuola Superiore Sant'Anna, Pisa, Italy

OPEN ACCESS

Edited by:

Christophe Godin,
Institut National de Recherche en
Informatique et en Automatique,
France

Reviewed by:

Stéphane Douady,
UMR7057 Laboratoire Matière et
Systèmes Complexes, France
Renaud Bastien,
Centre de Recherches
Interdisciplinaires, France

*Correspondence:

Daniele Agostinelli
daniele.agostinelli@sissa.it;
daniele.agostinelli@ubc.ca

† Present address:

Daniele Agostinelli,
Department of Mechanical
Engineering, University of British
Columbia, Vancouver, BC, Canada

Specialty section:

This article was submitted to
Plant Biophysics and Modeling,
a section of the journal
Frontiers in Plant Science

Received: 18 September 2020

Accepted: 17 February 2021

Published: 23 March 2021

Citation:

Agostinelli D, DeSimone A and
Noselli G (2021) Nutations in Plant
Shoots: Endogenous and Exogenous
Factors in the Presence of Mechanical
Deformations.
Front. Plant Sci. 12:608005.
doi: 10.3389/fpls.2021.608005

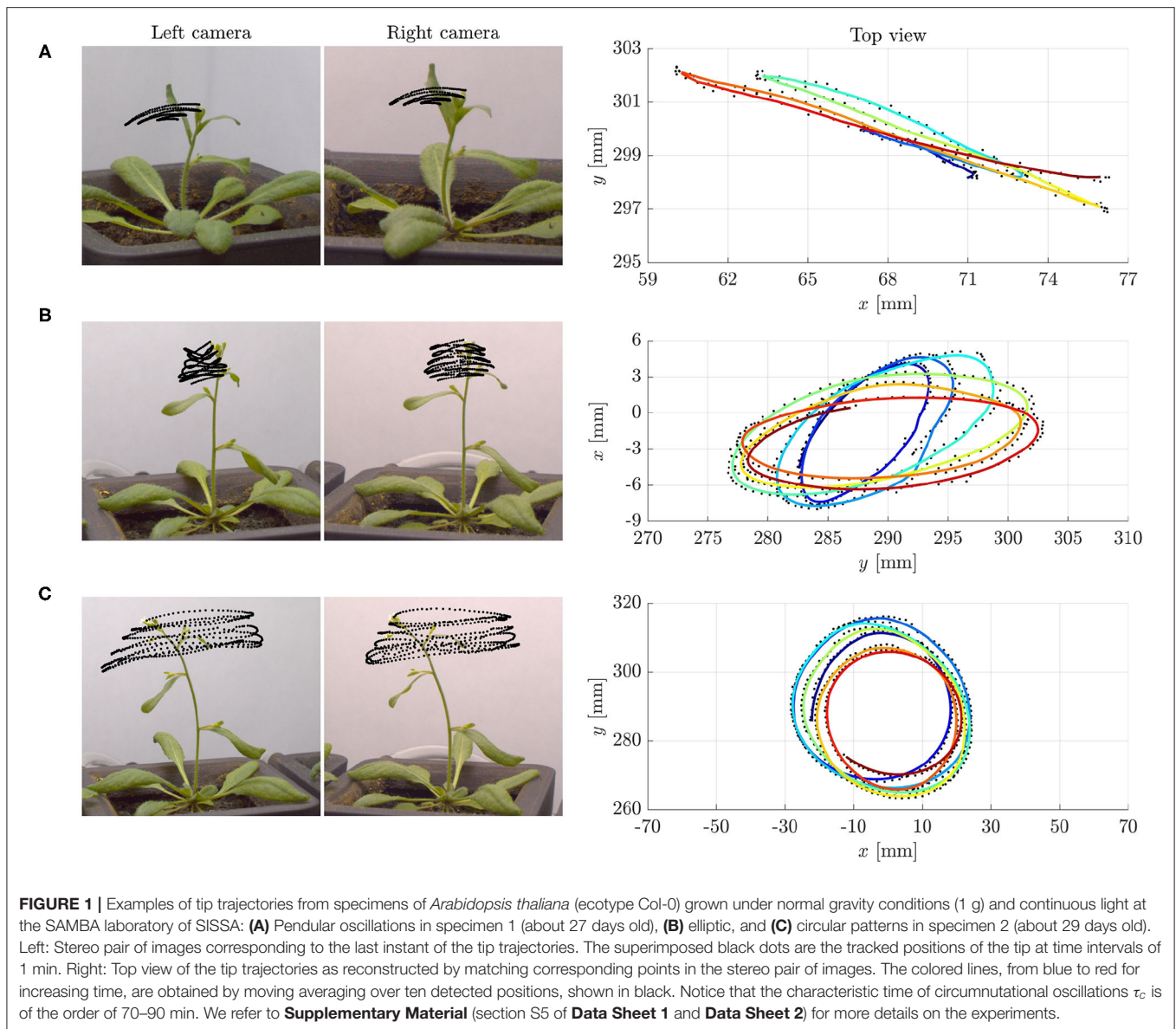
We present a three-dimensional morphoelastic rod model capable to describe the morphogenesis of growing plant shoots driven by differential growth. We discuss the evolution laws for endogenous oscillators, straightening mechanisms, and reorientations to directional cues, such as gravitropic reactions governed by the avalanche dynamics of statoliths. We use this model to investigate the role of elastic deflections due to gravity loading in circumnutating plant shoots. We show that, in the absence of endogenous cues, pendular and circular oscillations arise as a critical length is attained, thus suggesting the occurrence of an instability triggered by exogenous factors. When also oscillations due to endogenous cues are present, their weight relative to those associated with the instability varies in time as the shoot length and other biomechanical properties change. Thanks to the simultaneous occurrence of these two oscillatory mechanisms, we are able to reproduce a variety of complex behaviors, including trochoid-like patterns, which evolve into circular orbits as the shoot length increases, and the amplitude of the exogenous oscillations becomes dominant.

Keywords: plant morphogenesis, 3D morphoelastic rods, differential growth, circumnutation, two-oscillator hypothesis

1. INTRODUCTION

The extraordinary variety of movements in plants has fascinated scientists since the pioneering work by Darwin (1880), and is raising considerable and growing interest. Many essential functions involve passive conformational changes and active adaptation triggered by diverse conditions. Spectacular illustrations range from reproductive methods by explosive seed and pollen dispersal (Hofhuis et al., 2016), to nutrition and defense strategies, such as the snapping of *Venus flytrap* (Forterre et al., 2005) or the closing of *Mimosa Pudica*. This also includes the search for mechanical support by circumnutations of aerial organs in climbing plants, namely, pendular, elliptical or circular oscillatory movements. However, nutations occur also in some non-climbing plants, such as *Arabidopsis thaliana*, without any obvious purpose (see **Figure 1** and **Video 1**).

The nature of plant circumnutations has been intensively investigated over the last century, and this produced three main hypotheses (Stolarz, 2009). First, as already suggested by Darwin (1880), endogenous oscillators might drive the observed oscillatory movements, by internally regulating differential growth. Second, circumnutations might be the byproduct of posture control



mechanisms that overshoot the target equilibrium, due to delayed responses (Gradmann, 1922). Third, the previous two mechanisms might be combined in a “two-oscillator” hypothesis in which endogenous prescriptions and delayed responses coexist (Johnsson et al., 1999; Stolarz, 2009).

The overshooting hypothesis is typically based on externally driven feedback systems (of gravitropic, autotropic, phototropic, or other nature) and neglects mechanical (elastic) deformations of the plant organ. In this way, the role of elasticity in plant circumnutations remained relatively unexplored until a recent study showed that accounting for elastic deflections due to gravity loading enriches the scenario. Spontaneous oscillations might arise as system instabilities (bifurcations) when a loading parameter exceeds a critical value (Agostinelli et al., 2020b), similarly to dynamic instabilities (*flutter*) exhibited, e.g., by mechanical systems under nonconservative

loads (Bigoni and Noselli, 2011; Bigoni et al., 2018). However, such results are restricted to the two-dimensional case, and derive from a simplified analysis at constant length and without proprioceptive responses.

Plant circumnutations have often been studied by tracking the trajectory of the apical part of a growing shoot. It has also been recognized, however, that in order to relate these measurements to the inner mechanism of plants, the relation between the shape of the whole organ and the position of the apical tip needs to be resolved (Bastien and Meroz, 2016). It is then quite natural to ask the question whether light on such a relation can be shed by a model of the shoot as a growing rod, capable of deforming elastically under the action of external loads, and responding actively to external stimuli. To test this hypothesis, and building upon the theory of morphoelastic rods (Goriely, 2017), we propose in the present

study a three-dimensional model for growing plant shoots that includes gravitropic responses driven by the statoliths avalanche dynamics, proprioception, lignification, and also an endogenous oscillator. Our goal is to apply the model to the study of plant circumnutations, with a particular focus on the issue that has received least attention until now, namely, the role of elastic deformations in determining the observed movements.

We find that, in our model, elastic deformations significantly impact the growth regimes for which spontaneous (exogenous) oscillations arise in the absence of endogenous factors. Indeed, when all the biomechanical and growth parameters but the stiffness and the shoot length are fixed, there exists a critical length beyond which spontaneous oscillatory motions, representing a system instability due to the presence of gravity loading, become possible. Moreover, we show that when an endogenous factor is also present, the relative weight of endogenous versus exogenous mechanisms changes: as the shoot elongates, the oscillations associated with the instability mechanism become dominant over those of endogenous origin (see **Videos 2, 3**). In intermediate regimes, we find trochoid-like patterns that are reminiscent of the trajectories observed by Schuster and Engelmann (1997) in the hypocotyls of *A. thaliana*. In this way, the combination of endogenous and exogenous factors in the presence of mechanical (elastic) deformations might reproduce the observed variability of nutation patterns as a consequence of the existence of different regimes, and of their interplay. Therefore, the present study suggests that it may be worth re-examining the “two-oscillator hypothesis” from a renewed perspective, namely, by accounting for elastic deformations due to gravity loading.

2. MATERIALS AND METHODS

In this section we propose a 3D morphoelastic rod model to describe a growing plant shoot and we derive a reduced model for times that are short compared to those characterizing growth. Here we provide a minimal description of the model and we refer to **Supplementary Material** (section S1) for a detailed derivation of the proposed equations from a more general framework.

2.1. The Morphoelastic Rod Model for Growing Plant Shoots

We model a plant shoot as a growing, unshearable, and (elastically) inextensible elastic rod with circular cross section of radius r . This is a slender three-dimensional solid body that at time t occupies the cylindrical region surrounding a *centerline* $\mathbf{p}(s, t) \in \mathbb{R}^3$ where $s \in [0, \ell(t)]$ is the arc length parameter and identifies material cross sections, from the base, $s = 0$, to the apex, $s = \ell$. In order to describe the motion of the rod, we equip the centerline with an orthonormal basis of *directors* $\{\mathbf{d}_1(s, t), \mathbf{d}_2(s, t), \mathbf{d}_3(s, t)\}$, which define the orientation of each cross section. In particular, \mathbf{d}_1 and \mathbf{d}_2 identify two material fibers of the cross section, and $\mathbf{d}_3 := \mathbf{d}_1 \times \mathbf{d}_2$ is the unit vector normal to the cross section and tangent to the centerline, i.e., $\mathbf{d}_3 = \partial_s \mathbf{p}$ where ∂_s denotes the partial derivative with respect to s (see **Figure 2A**, Antman, 2005). The *Darboux vector* $\mathbf{u}(s, t)$

describes the way the directors \mathbf{d}_i vary along the rod through $\partial_s \mathbf{d}_j = \mathbf{u} \times \mathbf{d}_j$ for $j = 1, 2, 3$, and it encodes the bending and torsional deformations of the rod (see **Figure 2C**). The components $u_j := \mathbf{u} \cdot \mathbf{d}_j$, $j = 1, 2$, are called *flexural strains* as they define the bending of the rod about \mathbf{d}_1 and \mathbf{d}_2 , whereas $u_3 = \mathbf{u} \cdot \mathbf{d}_3$ is the *torsional strain*, as it defines the relative rotation about \mathbf{d}_3 between neighboring cross sections (Antman, 2005). At any time t , we reconstruct the rod—centerline and directors—corresponding to a Darboux vector \mathbf{u} by integrating the kinematic equations

$$\partial_s \mathbf{d}_j = \mathbf{u} \times \mathbf{d}_j \quad \text{for } j = 1, 2, 3, \quad \text{and} \quad \mathbf{d}_3 = \partial_s \mathbf{p}, \quad (1)$$

see **Figure 2C**.

The deformations encoded in \mathbf{u} result from both an elastic component due to external loads, and a spontaneous or intrinsic one (\mathbf{u}^* , see **Figure 2E**) associated with growth. In the absence of external loads, the Darboux vector results only from the intrinsic component (namely, $\mathbf{u} = \mathbf{u}^*$) and the spontaneous strains completely define the configuration of the rod through (1). We discuss first the intrinsic term, and then the elastic one.

We describe the subapical growth of the shoot as a stretch of the centerline with respect to a reference configuration that is parameterized by an arc length coordinate $S \in [0, \ell_0]$, where ℓ_0 is the plant length at initial time. We define the *stretch* as $\gamma := \partial_s s$ where $s(S, t)$ is the coordinate at time t of the material cross section identified by the parameter S in the reference configuration. Then we define the *true strain* as $\varepsilon := \ln \gamma$, so that the *relative elemental growth rate* (REGR) introduced by Erickson and Sax (1956) reduces to $\dot{\varepsilon} = \partial_t \gamma / \gamma$, where a superimposed dot denotes the material time derivative. Since such a quantity can be experimentally measured by tracking material markers along the organ (Maksymowych et al., 1985; Berg and Peacock, 1992; Mullen et al., 1998; van der Wee et al., 2003; Hall and Ellis, 2012; Phyto et al., 2017), we prescribe a function $\text{REGR}(s, t)$, vanishing outside the elongating zone of length ℓ_g , i.e., $[\ell(t) - \ell_g, \ell(t)]$, and such that $\dot{\varepsilon} = \text{REGR}$. Consequently, subapical growth is governed by two coupled PDEs, namely,

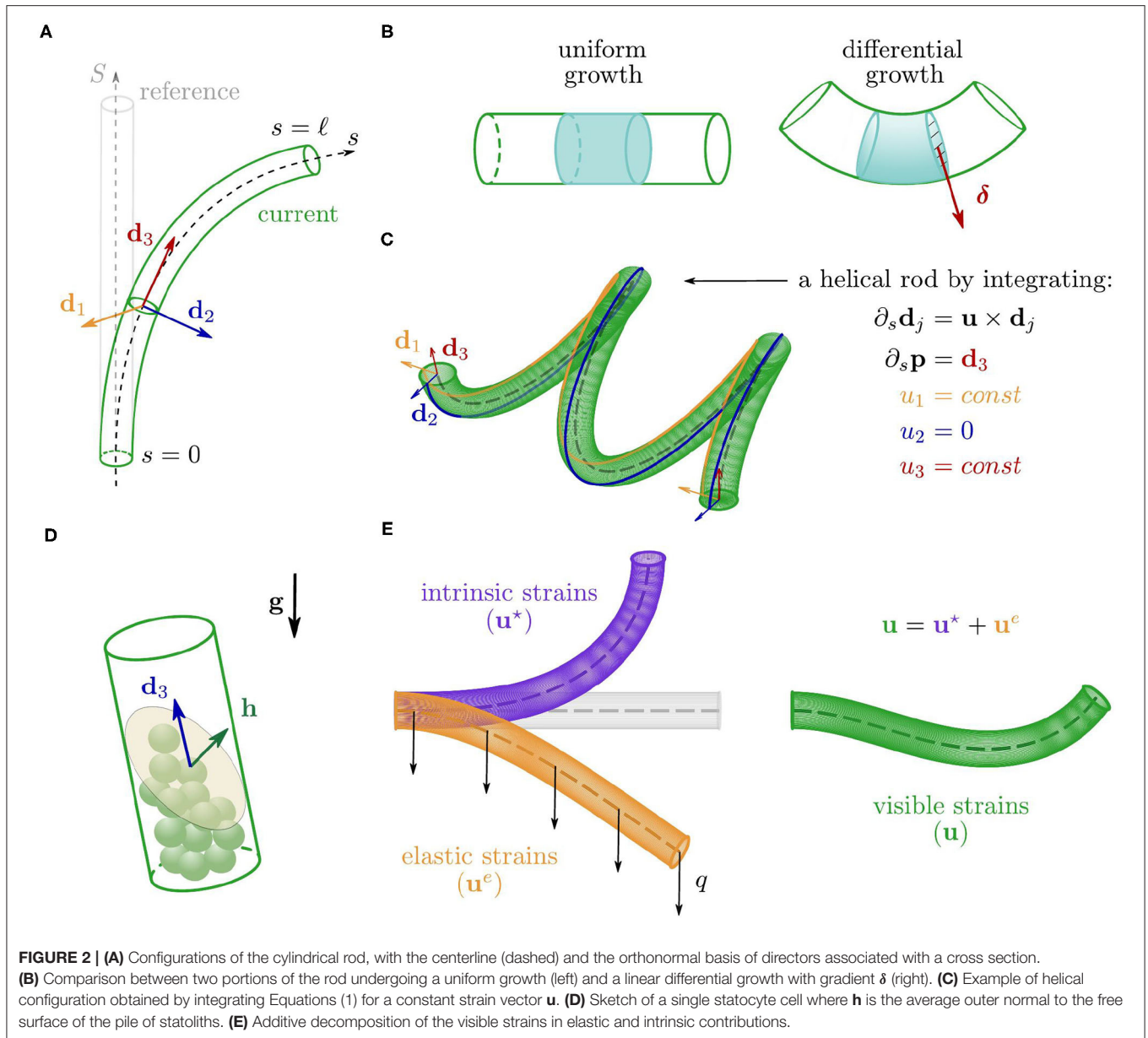
$$\frac{1}{\gamma} \frac{\partial \gamma}{\partial t} = \text{REGR} \quad \text{and} \quad \gamma = \frac{\partial s}{\partial S}, \quad (2)$$

to be solved for $S \in [0, \ell_0]$ and $t \geq 0$, with initial condition $\gamma(\cdot, 0) \equiv 1$ and fixed boundary datum $s(0, \cdot) \equiv 0$. Following previous studies (Bastien et al., 2014; Chelakkot and Mahadevan, 2017), among the possible choices (Agostinelli et al., in press), we use a piecewise constant growth function, namely,

$$\text{REGR}(S, t) = \begin{cases} 0 & \text{if } s(S, t) \leq \ell(t) - \ell_g, \\ \frac{1}{\tau_g} & \text{if } s(S, t) > \ell(t) - \ell_g, \end{cases} \quad (3)$$

where $\tau_g > 0$ is the characteristic growth time. Problem (2)–(3) has an analytical solution $s(S, t)$, and the shoot length $\ell(t)$ grows linearly in time, attaining the growth length ℓ_g (see **Figure 3**).

While growing, the shoot evolves and adapts its shape by means of a spatially nonhomogeneous growth rate of the cross section. This morphing mechanism, referred to as *differential*



growth, allows the plant to accommodate to a variety of stimuli. We assume that the organ radius r is small enough to justify a linearization about the center of the cross section, leading to a growth rate that has a linear profile with gradient δ , which relates to the spontaneous strains as follows

$$\delta(s, t) = \dot{u}_1^*(s, t)\mathbf{d}_2(s, t) - \dot{u}_2^*(s, t)\mathbf{d}_1(s, t), \quad (4)$$

where u_j^* are the components of \mathbf{u}^* with respect to the local basis $\{\mathbf{d}_j\}$, i.e., $u_j^* := \mathbf{u}^* \cdot \mathbf{d}_j$, for $j = 1, 2, 3$. Equation (4) reveals that differential growth governs the evolution of the spontaneous strains, u_j^* . Indeed, the growth gradient δ defines the direction along which the strain rate (or REGR) is linearly distributed on the cross section (see Figure 2B), thus determining the rates of the flexural strains, \dot{u}_1^* and \dot{u}_2^* . Here we assume that $u_3^* \equiv 0$,

even though this torsional strain could play a crucial role in other growth mechanisms, such as those observed in twining plants. In this study, we consider three possible drivers for differential growth: an endogenous oscillator, gravitropic responses, and proprioception. In the following, we discuss the evolution laws of the spontaneous strains as individually produced by each of these mechanisms.

1. *Endogenous oscillator.* Several studies on plant growth and nutations have revealed a strong correlation between oscillatory movements and biological rhythms, thus supporting the Darwinian concept of *internal oscillator* (Berg and Peacock, 1992; Schuster and Engelmann, 1997; Shabala and Newman, 1997; Buda et al., 2003; Shabala, 2003; Niinuma et al., 2005; Mugnai et al., 2015). Here, following previous approaches (Bastien and Meroz, 2016; Porat et al., 2020), we

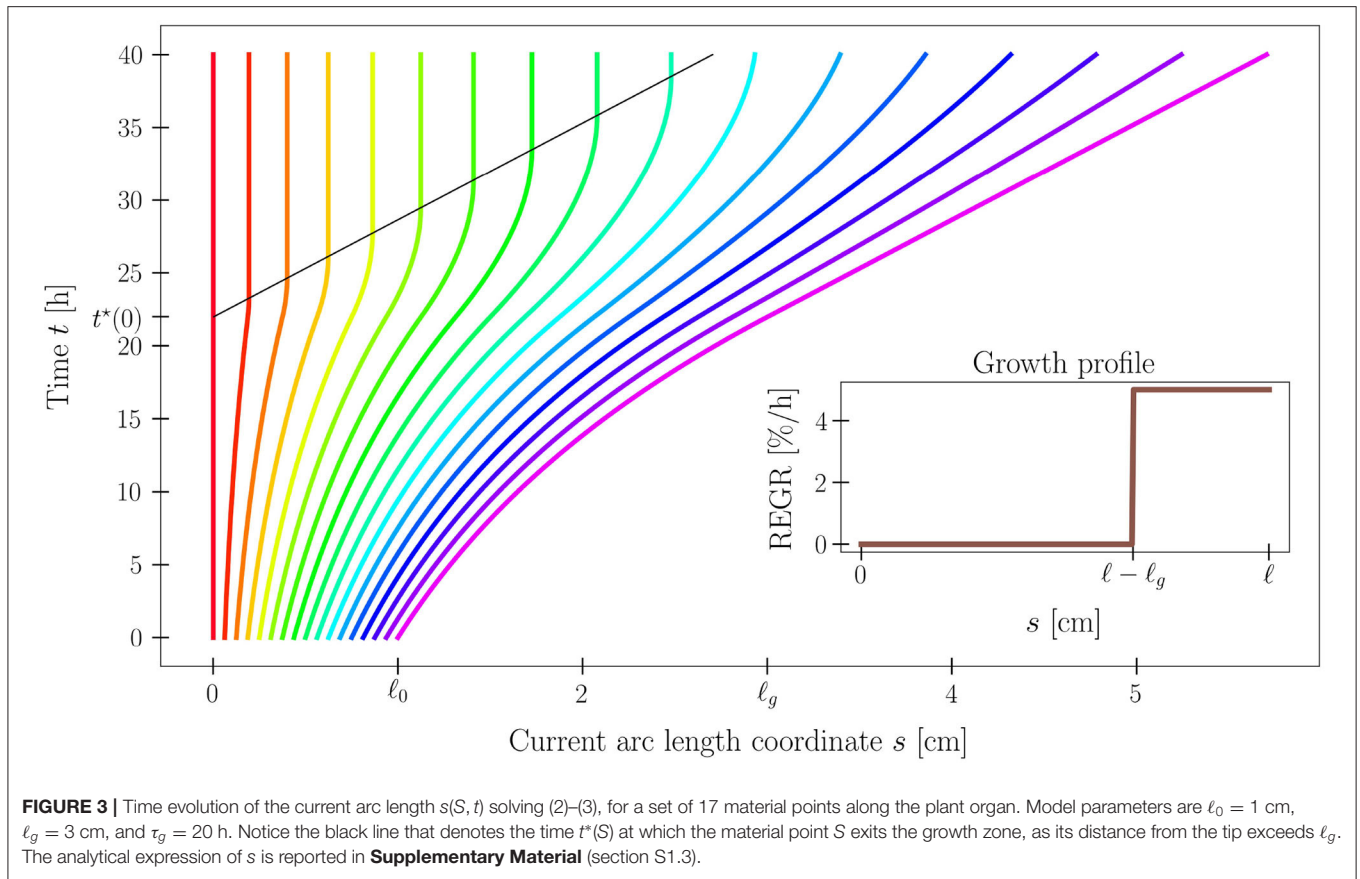


FIGURE 3 | Time evolution of the current arc length $s(S, t)$ solving (2)–(3), for a set of 17 material points along the plant organ. Model parameters are $\ell_0 = 1$ cm, $\ell_g = 3$ cm, and $\tau_g = 20$ h. Notice the black line that denotes the time $t^*(S)$ at which the material point S exits the growth zone, as its distance from the tip exceeds ℓ_g . The analytical expression of s is reported in **Supplementary Material** (section S1.3).

implement a spatially uniform time-harmonic oscillator with period τ_e , namely,

$$\dot{u}_1^*(s, t) = \alpha \frac{\dot{\epsilon}(s, t)}{r} \cos(2\pi t/\tau_e), \quad (5a)$$

$$\dot{u}_2^*(s, t) = \alpha \frac{\dot{\epsilon}(s, t)}{r} \sin(2\pi t/\tau_e), \quad (5b)$$

where α is a nonnegative dimensionless sensitivity associated with the endogenous cues.

2. **Gravitropic reactions.** Plant organs sense gravity through the sedimentation of starch-filled plastids, called *statoliths*, into specialized cells, called *statocytes*, which are found along the shoot growing zone and in the root caps (Chauvet et al., 2019; Nakamura et al., 2019). By extending the approach taken by Chauvet et al. (2019) to the three-dimensional case, we model the statoliths free surface as a plane with normal \mathbf{h} , whose dynamics is a viscous relaxation to $-\mathbf{g}$ (see **Figure 2D**). As shown in **Supplementary Material** (section S2), the time evolution of \mathbf{h} is governed by

$$\sum_j \dot{h}_j \mathbf{d}_j = \frac{1}{\tau_a} \mathbf{h} \times (\mathbf{h} \times \mathbf{g}), \quad (6)$$

where τ_a is the characteristic time for the statoliths avalanche dynamics and $h_j := \mathbf{h} \cdot \mathbf{d}_j$. Equation (6) shows that $\mathbf{h} =$

$-\mathbf{g}$ provides an equilibrium configuration for the statoliths. Then we implement a gravitropic contribution to the growth gradient to align the axis of the organ with the perceived gravity vector \mathbf{h} as

$$\dot{u}_1^*(s, t) = -\beta \frac{\dot{\epsilon}(s, t)}{r\tau_m} \int_{-\infty}^{t-\tau_r} e^{-\frac{1}{\tau_m}(t-\tau_r-\tau)} h_2(s, \tau) d\tau, \quad (7a)$$

$$\dot{u}_2^*(s, t) = \beta \frac{\dot{\epsilon}(s, t)}{r\tau_m} \int_{-\infty}^{t-\tau_r} e^{-\frac{1}{\tau_m}(t-\tau_r-\tau)} h_1(s, \tau) d\tau, \quad (7b)$$

where β is a nonnegative dimensionless constant expressing the organ sensitivity to gravi-stimulation, whereas τ_m and τ_r are the memory and reaction times of the gravitropic response, respectively. Equations (7) account for memory and delay effects by means of an integration over time of the stimulus, properly weighted by an exponential function (Israelsson and Johnsson, 1967; Chauvet et al., 2019; Agostinelli et al., 2020b). If we confine the rod to a plane, Equations (7) reduce to the extension of Sach's sine law provided by Chauvet et al. (2019).

3. **Straightening mechanisms (or proprioception).** Some experiments have pointed out the existence of an independent straightening mechanism, often referred to as proprioception, autotropism, or autostraightening, which is triggered by bending of the organ (Okamoto et al., 2015). Following Bastien et al. (2014) and Bastien and Meroz (2016), we assume that such a straightening response is driven by the

geometric curvature of the organ, i.e., $\kappa = (u_1^2 + u_2^2)^{1/2}$, thus producing a growth gradient parallel to the visible normal vector $\mathbf{v} := \kappa^{-1} \partial_s \mathbf{d}_3$. This leads to the evolution laws

$$\dot{u}_1^*(s, t) = -\eta \frac{\dot{\epsilon}(s, t)}{\bar{\tau}_m} \int_{-\infty}^{t-\bar{\tau}_r} e^{-\frac{1}{\bar{\tau}_m}(t-\bar{\tau}_r-\tau)} u_1(s, \tau) d\tau, \quad (8a)$$

$$\dot{u}_2^*(s, t) = -\eta \frac{\dot{\epsilon}(s, t)}{\bar{\tau}_m} \int_{-\infty}^{t-\bar{\tau}_r} e^{-\frac{1}{\bar{\tau}_m}(t-\bar{\tau}_r-\tau)} u_2(s, \tau) d\tau, \quad (8b)$$

where η is a nonnegative dimensionless constant for the proprioceptive sensitivity of the organ, whereas $\bar{\tau}_m$ and $\bar{\tau}_r$ are the memory and reaction times of the straightening mechanism, respectively. As for gravitropism, we model proprioception by a distributed delay with an exponential kernel.

We assume the existence of separate signaling pathways for different simultaneous stimuli so that we obtain the overall evolution laws for the spontaneous strains by summing the corresponding right-hand sides of Equations (5), (7), and (8). In fact, studies show interactions between different tropisms (Correll and Kiss, 2002), but we neglect them because the microscopic mechanisms and pathways for this cross-talk remain unknown for many plant responses (Okamoto et al., 2015; Su et al., 2017; Levernier et al., 2021).

For both gravitropism and proprioception, we provide a phenomenological description of memory and delay by integrating the stimuli over time, weighted by an exponential kernel function [cf. Equations (7)–(8)]. Even though we could implement more realistic models by fitting the kernel function with suitable experiments (Meroz et al., 2019), or by solving for the hormone transport (Moulton et al., 2020; Levernier et al., 2021), we opt for parsimony over complexity in order to capture the phenomenon while making it mathematically tractable.

Finally, we adapt this framework to include elastic deformations due to gravity loading. In this case, the configuration of the rod results from two contributions: elastic and intrinsic strains (see **Figure 2E**). The additive formula captures the simplest form consistent with this idea, so that

$$u_j = u_j^* + u_j^e \quad \text{for } j = 1, 2, 3, \quad (9)$$

where u_j^* are the spontaneous strains that evolve to accommodate to external cues, as previously discussed, whereas u_j^e are the elastic strains due to bending and twisting moments generated by the gravity loading. In particular, we assume

$$u_j^e = \frac{m_j}{K_j} \quad \text{for } j = 1, 2, 3, \quad (10)$$

where K_j and $m_j := \mathbf{m} \cdot \mathbf{d}_j$ are the bending and torsional stiffnesses and moments, respectively, and \mathbf{m} is the contact couple. Under the assumption that the time scale for mechanical equilibrium is much shorter than any biological time scale of the plant, we

determine the contact couple \mathbf{m} by solving the two fundamental equations of mechanical balance, i.e.,

$$\partial_s \mathbf{n}(s, t) + \mathbf{f}(s, t) = \mathbf{0}, \quad \partial_s \mathbf{m}(s, t) + \partial_s \mathbf{p}(s, t) \times \mathbf{n}(s, t) = \mathbf{0}, \quad (11)$$

where \mathbf{n} is the contact force acting on the cross section, and \mathbf{f} is the body force per unit current length. Equations (11) derive from the balance laws of linear and angular momentum under the assumption of negligible inertia effects, and they are referred to as the *Kirchhoff equations* (Antman, 2005; Goriely, 2017). More specifically, we assume that the shoot carries a uniform distributed gravity load $q = \rho g A \geq 0$, where ρ is the mass density, $A = \pi r^2$ is the cross-sectional area, and g is the gravitational acceleration so that $\mathbf{f} = q \mathbf{g}$. Since the apical end is free, the boundary conditions associated with Equations (11) read $\mathbf{n}(\ell(t), t) = \mathbf{0}$ and $\mathbf{m}(\ell(t), t) = \mathbf{0}$. Then, the first equation can be integrated to get $\mathbf{n} = q(\ell(t) - s) \mathbf{g}$ and we are left with

$$\partial_s \mathbf{m}(s, t) = q(\ell(t) - s) \mathbf{g} \times \mathbf{d}_3(s, t), \quad (12)$$

together with the boundary condition $\mathbf{m}(\ell(t), t) = \mathbf{0}$. In principle, once \mathbf{m} is known, using the constitutive Equations (10), one could express the strains as $\mathbf{u} = \mathbf{u}^* + \mathbf{u}^e$ and obtain, by integration of the kinematic Equations (1), the configuration of the rod. However, Equation (12) cannot be solved independently, since it contains the unknown tangent \mathbf{d}_3 and determining the visible configuration of the rod requires, in fact, the solution of a coupled nonlinear system. In the case $\mathbf{h} = -\mathbf{g}$ of fast statoliths avalanche dynamics, these are 24 scalar equations [i.e., (1), (9), (10), (12), and the three equations determining the evolution of u_j^*] in 24 scalar variables (the components of \mathbf{p} , \mathbf{d}_1 , \mathbf{d}_2 , \mathbf{d}_3 , \mathbf{u} , \mathbf{u}^* , \mathbf{u}^e , and \mathbf{m}). Neglecting elasticity, this reduces to 15 equations in 15 scalar variables (the components of \mathbf{p} , \mathbf{d}_1 , \mathbf{d}_2 , \mathbf{d}_3 , and $\mathbf{u} = \mathbf{u}^*$).

The stiffnesses K_j depend on the cross section geometry. Even though elliptic cross sections might provide a better approximation (Paul-Victor and Rowe, 2011), we opt for the simpler assumption of circular cross section of radius r . In this case, $K_1 = K_2 = EI$ where E is the Young's modulus and $I = \pi r^4/4$ is the second moment of inertia, and $K_3 = \mu J$ where $J = 2I$ and $\mu = 2E(1 + \nu)$ is the shear modulus determined by the Poisson's ratio ν (Antman, 2005; Goriely, 2017). Since we expect lignification processes to play a crucial role in the mechanics of the organ, over a long period of time, we include also a rod stiffening, by adapting the approach of Chelakkot and Mahadevan (2017); in particular, we assume the Young's modulus to evolve in time according to

$$E(S, t) = E_1 - (E_1 - E_0) e^{-\max\{0, t-t^*(S)\}/\tau_\ell}, \quad (13)$$

where $t^*(S)$ is the time at which the material point S exits the growth zone, τ_ℓ is the lignification characteristic time, whereas E_0 and E_1 are the minimum and maximum values of the Young's modulus, respectively.

2.2. The Reduced Model for Short Times

The rod model introduced in section 2.1 presents some difficulties for a theoretical study but we can derive a reduced

TABLE 1 | Summary of model parameters and respective order of magnitude of their values.

Parameter	Description	Value	References
Sensitivities for differential growth			
α	Sensitivity to endogenous cues	0 – 1	Assumed
β	Gravitropic sensitivity	0.8	Chauvet et al. (2019)
η	Proprioceptive sensitivity	20	Assumed
Characteristic times			
τ_a	Time for statoliths avalanche	2 min	Chauvet et al. (2019)
τ_e	Period of endogenous oscillations	20 min	Assumed
τ_m	Gravitropic memory time	12 min	Chauvet et al. (2019)
$\bar{\tau}_m$	Proprioceptive memory time	12 min	Assumed
τ_r	Gravitropic reaction time	12 min	Chauvet et al. (2019)
$\bar{\tau}_r$	Proprioceptive reaction time	12 min	Assumed
τ_g	Growth time	20 – 40 h	Chauvet et al. (2019), Hall and Ellis (2012), and Phyo et al. (2017)
τ_ℓ	Lignification time	6 d	Assumed
Morphological and biomechanical parameters			
r	Radius of the cross section	0.5 mm	Paul-Victor and Rowe (2011)
ℓ_g	Growth zone	4 – 7 cm	Hall and Ellis (2012)
ν	Poisson's ratio	0.5	Assumed
ρ	Mass density	10^3 Kg m^{-3}	Chelakkot and Mahadevan (2017)
E_0	Initial Young's modulus	10 MPa	Chelakkot and Mahadevan (2017)
E_1/E_0	Stiffening ratio due to lignification	200	Assumed

version for a linearized analysis of processes that are much faster than growth (and hence lignification) and much slower than the statoliths dynamics. Indeed—for short time periods—we can neglect changes in length (i.e., $\ell \approx \ell_0 \leq \ell_g$), and in the Young's modulus (i.e., $E \approx E_0$), as growth and lignification are slow; in this case, current and reference arc lengths coincide such that material time derivatives reduce to standard time derivatives. Moreover, we can disregard the transient in the statoliths sedimentation and assume that, at all times, the statoliths free surface is a plane normal to the gravity vector (i.e., $\mathbf{h} = -\mathbf{g}$), as its dynamics is fast. We report the equations of such a model in **Supplementary Material** (section S3.3), together with their linearization for the stability analysis.

3. RESULTS

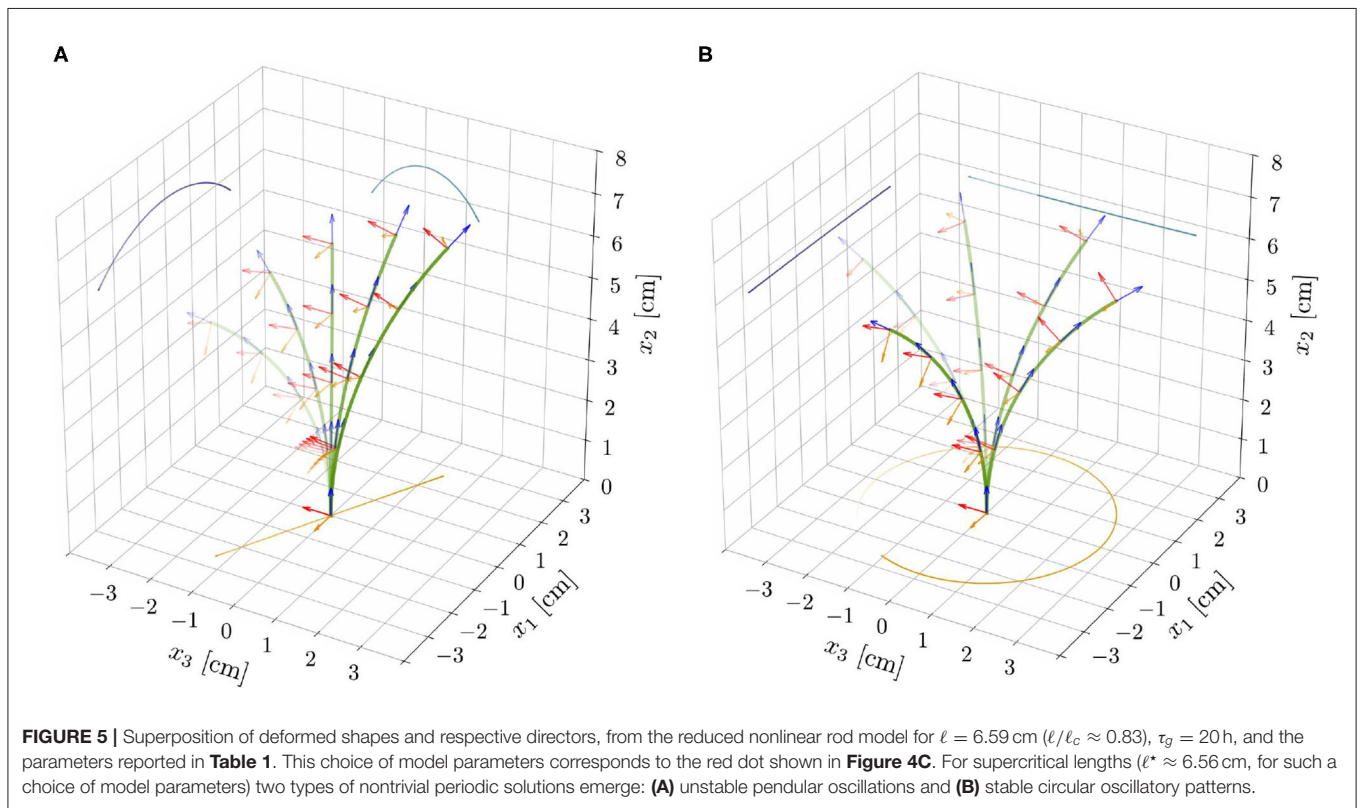
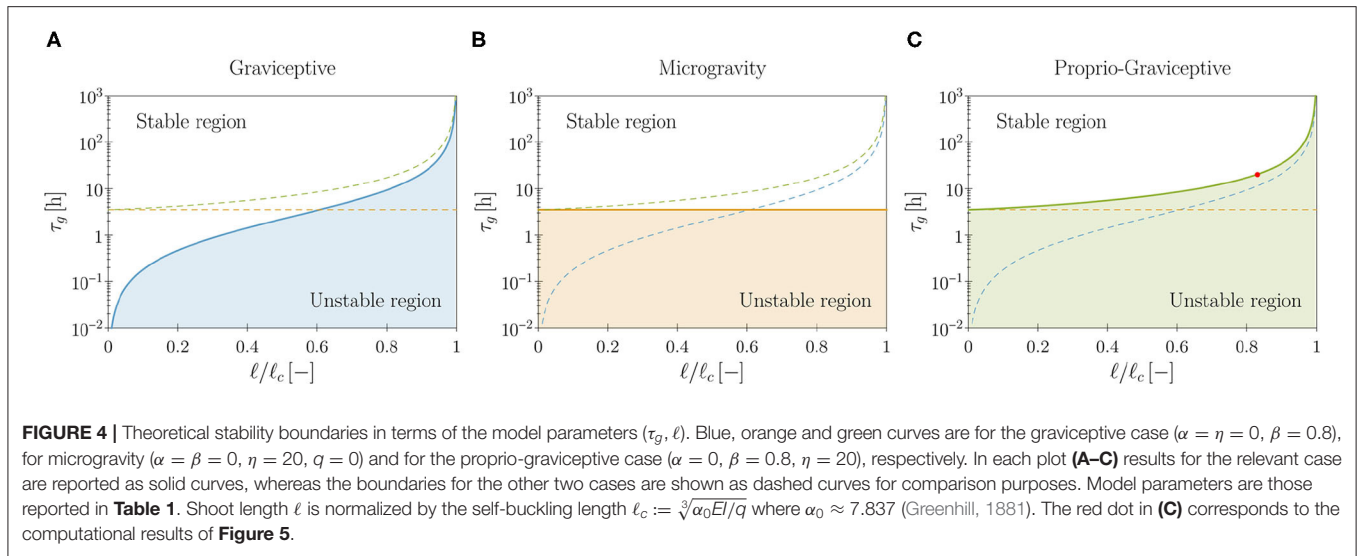
In this section we present the results of our study of plant circumnutations based on the models proposed in section 2, and for the relevant parameters listed in **Table 1**. The reduced model reveals the possible emergence of spontaneous oscillations associated with gravitropic and proprioceptive responses as a mechanism independent of endogenous oscillators; the onset of these spontaneous oscillations is crucially affected by elasticity. The full model shows the effects of shoot elongation during growth, and confirms the potential key role of elasticity

in circumnutations: a loading parameter, such as the shoot length, determines the relative importance between the two oscillatory mechanisms.

3.1. The Regime of Short Times

As detailed in **Supplementary Material** (section S3), a linearized analysis of the reduced model reveals the change in the stability character of the upright trivial equilibrium when a loading parameter exceeds a critical value. In the nonlinear model, this event corresponds to the emergence of periodic, oscillatory movements, as found numerically by means of the computational model described in **Supplementary Material** (section S4). We investigate the role of elasticity in determining the stability thresholds for the onset of spontaneous oscillations in the following different scenarios.

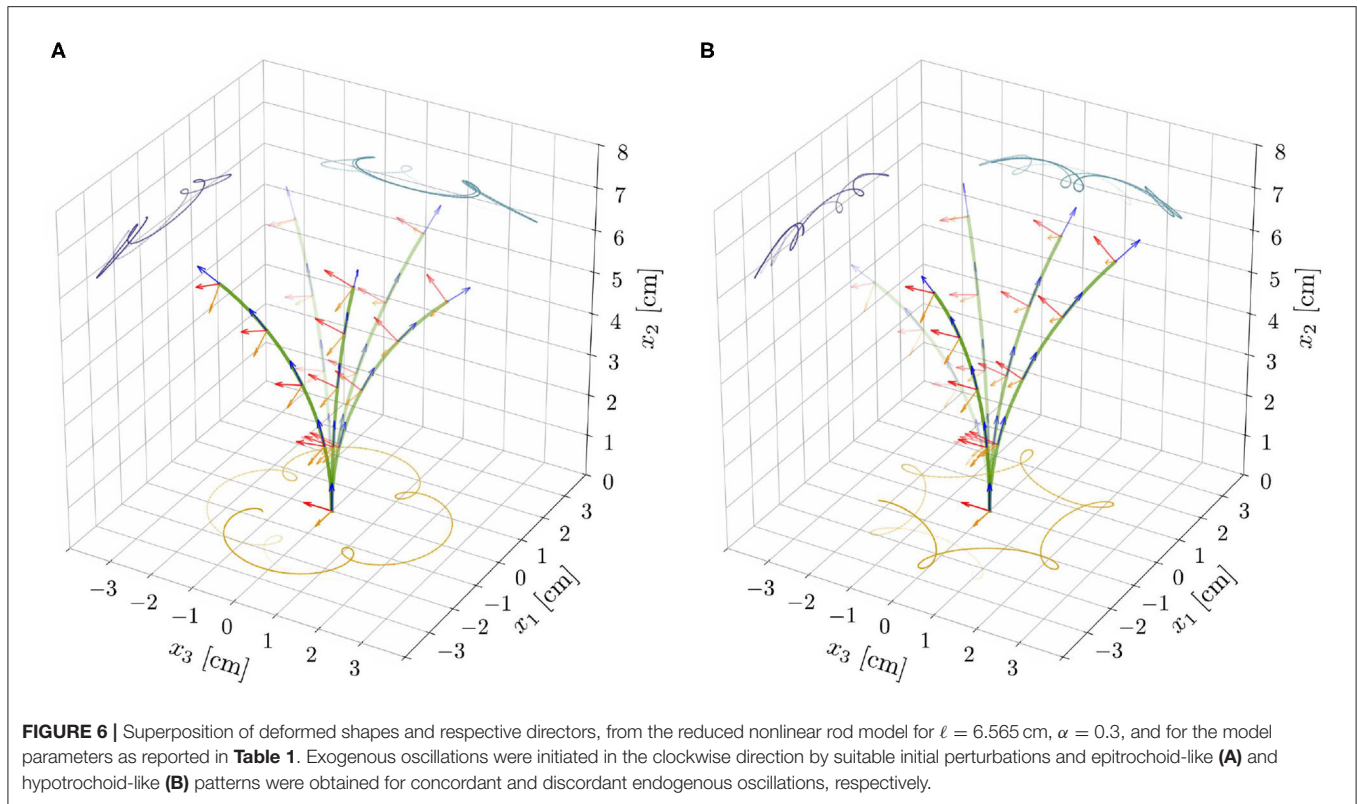
- 1. Gravitropic case:** $\alpha = \eta = 0$ and $\beta > 0$. In the absence of both endogenous cues ($\alpha = 0$) and straightening mechanisms ($\eta = 0$), the straight equilibrium configuration becomes unstable as the plant shoot attains a critical length (see **Supplementary Material**, section S3.3.1). We report in **Figure 4A** the stability boundary for the system in terms of the characteristic time of growth τ_g and the shoot length ℓ . In the unstable region we find pendular oscillations (already observed in the planar version of the present model, Agostinelli et al., 2020b) and new three-dimensional circular trajectories, which emerge as limit cycles of the nonlinear model. In other terms, spontaneous—pendular and circular—oscillations emerge when the shoot is longer than a critical threshold, fixed all other parameters. In this case, the role of elasticity is sharp: no oscillations occur in the absence of elastic deflections due to gravity loading. Indeed, neglecting elasticity means that $\ell_c \rightarrow \infty$ (either by letting the rod stiffness tend to infinity or by removing the gravity loading), and in this limit the plant shoot is always stable, irrespective of τ_g (see **Figure 4A**).
- 2. Microgravity:** $\alpha = \beta = 0$, $\eta > 0$, and $q = 0$. As an intermediate case study, we analyze the model in microgravity conditions by discarding the twofold action of gravity: gravitropic reactions do not occur and the plant is weightless. In this way we isolate the effect of proprioceptive responses. In agreement with previous studies (Johnsson et al., 1999) we find that proprioception alone might induce spontaneous oscillations, which occur at a critical value of τ_g that is independent of the shoot length (see **Figure 4B** and **Supplementary Material**, section S3.3.2). These oscillations lack elastic deformations, as the plant is weightless. For the model parameters of **Table 1**, we find a critical value of approximately 3.5 h. However, this seems to be out of the range of experimental observations, thus suggesting that the persistence of oscillations in microgravity might have an endogenous origin (Johnsson et al., 2009; Kobayashi et al., 2019).
- 3. Proprio-gravitropic case:** $\alpha = 0$ and $\beta, \eta > 0$. Finally, we extend the analysis to the case in which proprioception and gravitropism coexist. We observe that—similarly to the case of microgravity but contrary to the gravitropic



case—oscillations are possible whenever τ_g is less than the critical value of 3.5 h, thanks to proprioception. However, elastic deformations significantly impact the stability threshold (see **Figure 4C** and **Supplementary Material**, section S3.3.3). Indeed, this depends on ℓ/ℓ_c , as found for the gravitropic case. A numerical study of the nonlinear regime reveals the occurrence of pendular and circular limit cycles in the unstable region (see **Figure 5** and **Video 4**). Further, for a given τ_g , proprioception lowers

the critical length with respect to the graviceptive case, provided that the delay $\bar{\tau}_r$ and the memory time $\bar{\tau}_m$ are sufficiently large (see **Supplementary Material**, section S3.3.3).

These results confirm the existing hypothesis that exogenous, spontaneous oscillations might occur even in the absence of endogenous oscillators (Mugnai et al., 2015). However, experiments might lead to erroneous conclusions when



compared to theoretical predictions from models that neglect elasticity, as this strongly influences the onset of oscillations.

Finally, we investigate how an endogenous, time-harmonic oscillator of period τ_e affects the spontaneous oscillations that we observed in the proprio-graviceptive case. To this aim, we explored the nonlinear reduced model with $\alpha, \beta, \eta > 0$, by means of the computational implementation described in **Supplementary Material** (section S4). In the stable region, the intrinsic oscillator dominates the dynamics and the solutions ultimately converge to motions of period τ_e . On the contrary, in the unstable region, the tip traces epitrochoid-like or hypotrochoid-like patterns, depending on whether the rotational directions of the two oscillatory mechanisms are concordant or discordant, respectively (see **Figure 6** and **Videos 5, 6**). We observe inexact periodic trochoids, as the ratio between the two periods that come into play—the one of the internal oscillator, τ_e , and the one associated with the limit cycle—is typically an irrational number.

3.2. The Role of Plant Shoot Elongation

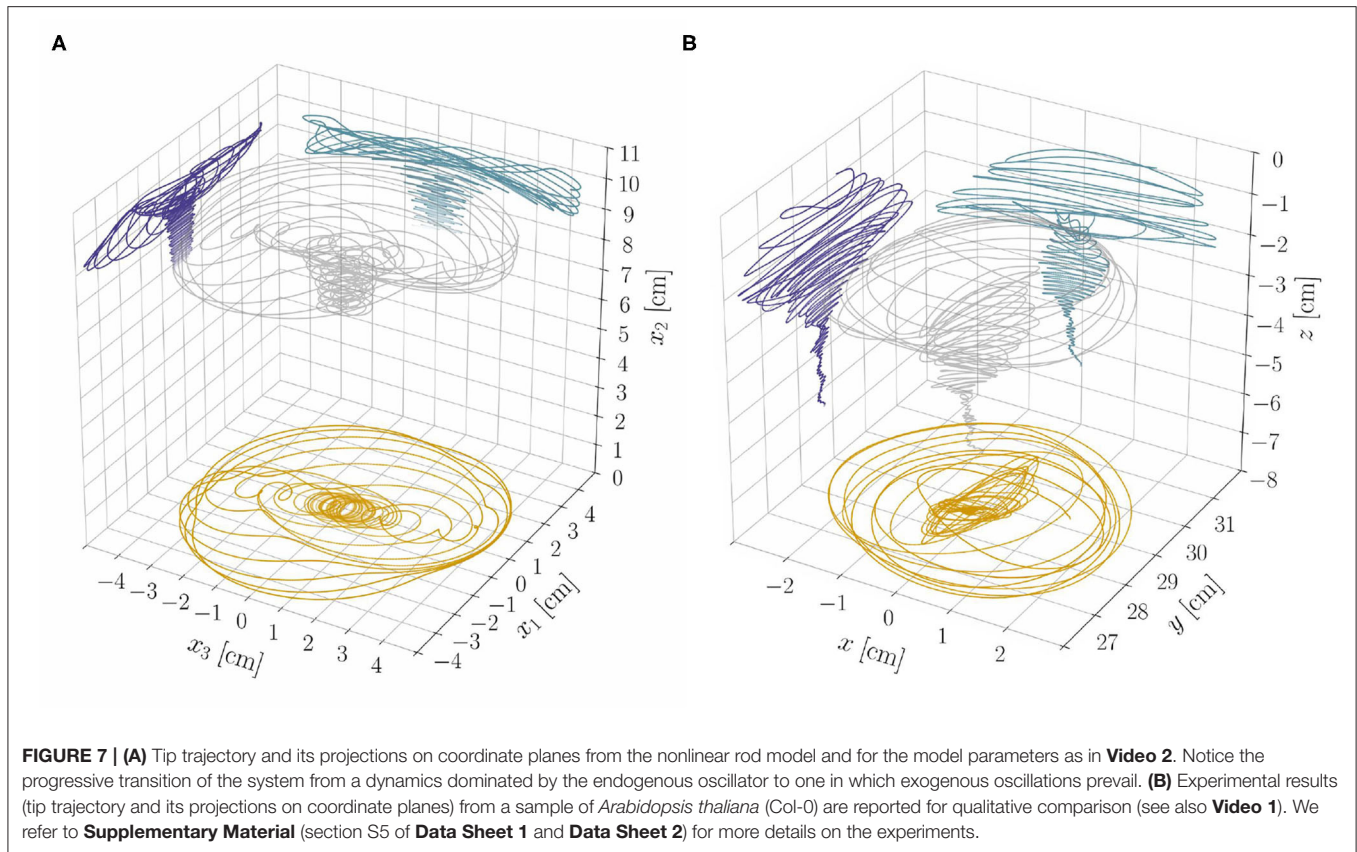
The results from the reduced model, at constant length, provide insight on the dynamics of the full model, which accounts for length changes, lignification processes, and statoliths dynamics. From section 3.1, we expect exogenous oscillations to arise once a critical length ℓ^* is attained, while all other parameters are fixed. Indeed, we find numerically (see **Supplementary Material**, section S4) that the relative

weight of the two oscillatory mechanisms—endogenous and exogenous—changes and affects the resulting dynamics as the shoot elongates. The system gradually transitions from a dynamics mainly characterized by endogenous oscillations in the subcritical, stable regime ($\ell < \ell^*$) to one in which exogenous oscillations dominate in the supercritical, unstable regime ($\ell > \ell^*$). Trochoid-like patterns appear in the intermediate regime (see **Figure 7A** and the **Videos 2, 3**).

Elasticity crucially influences the transition from one dynamics to the other, which generates different nutation patterns at different stages of growth of the same plant. To assess the plausibility of these theoretical findings, as a proof of principle, we performed some qualitative experimental observations of a plant exhibiting different nutation patterns at different growth stages. We report in **Figure 7B** the three-dimensional tip trajectory from a specimen of *A. thaliana*, and refer to **Supplementary Material** (section S5) for details on the experimental procedures.

4. DISCUSSION

In this study we proposed a new three-dimensional morphoelastic rod model capable of describing the motion of growing plant shoots, which accommodates an inherent straightening mechanism (proprioception), gravitropic responses, and an endogenous oscillator. This model generalizes



existing approaches in the literature (Bastien et al., 2014; Bastien and Meroz, 2016; Chelakkot and Mahadevan, 2017; Chauvet et al., 2019; Meroz et al., 2019; Agostinelli et al., 2020b; Porat et al., 2020; Tsugawa et al., 2020), by simultaneously accounting for the three-dimensionality of the shoot and the elastic deformations due to gravity loading. We intended this model as a test bed for different hypotheses about circumnutations in plant shoots, but it might be informative for other biological aspects or even in the context of bioinspired soft robotics, which recently started drawing inspiration from the plant kingdom to conceive and design innovative adaptable robots (Mazzolai, 2017).

Since the first experimental observations of plant circumnutations, a long-lasting debate produced three main theories for their nature: the existence of an endogenous oscillator (Darwin, 1880), a gravitropic feedback oscillator (Gradmann, 1922), or a combination of the two (Johnsson et al., 1999; Stolarz, 2009). Previous analyses of these theories disregarded elastic deflections due to gravity loading, which however may affect in a relevant way the mechanical stability of the biological system. Indeed, we showed that in our model the onset of exogenous oscillations largely depends on elasticity, as the system suffers an instability when a loading parameter, such as the shoot length, exceeds a critical threshold. In the presence of an endogenous oscillator, the relative amplitude of the two mechanisms varies in time: endogenous oscillations prevail in the subcritical, stable regime

of short shoots, while the exogenous ones dominate the supercritical, unstable regime of long shoots; in the intermediate, transient regime, the two competing oscillations can reproduce trochoid-like patterns (for which Schuster and Engelmann, 1997 provided experimental evidence). Interestingly, Darwin (1880) described a similar dynamics: “[...] *climbing plants whilst young circumnutate in the ordinary manner, but as soon as the stem has grown to a certain height, which is different for different species, it elongates rapidly, and now the amplitude of the circumnutating movement is immensely increased, evidently to favor the stem catching hold of a support* [...].” As a further proof of concept, we observed experimentally the transitions between different patterns and amplitude on the primary inflorescence of a specimen of *A. thaliana* Col-0 growing under continuous light (see **Figure 7B** and **Video 1**).

The reality of plant circumnutations is more complex than our simple modeling assumptions, and our theoretical predictions require a thorough quantitative assessment in comparison with experimental observations. However, we believe that this study provides the possibility to reinterpret the “two-oscillator hypothesis” and the vast existing experimental literature from a renewed perspective. Our results suggest the potential role of elasticity in circumnutations and provide a minimal mechanism/hypothesis that might account for the variability of the patterns and amplitudes of observed nutations, not only across different plant species and specimens but also at different stages of growth of the same plant.

DATA AVAILABILITY STATEMENT

The experimental data presented in this article are accessible as Supplementary Material at: <https://www.frontiersin.org/articles/10.3389/fpls.2021.608005/full#supplementary-material>. For simulations, the Python codes based on the FEniCS Project Version 2019.1.0 (Logg et al., 2012) are available at: <https://github.com/mathLab/MorphoelasticRod>.

AUTHOR CONTRIBUTIONS

All authors conceived the study, contributed to the theoretical analysis, and wrote the manuscript. GN and DA performed the experiments. DA analyzed the data, wrote the code, and carried out numerical computations. All authors gave final approval for publication and agree to be held accountable for the work performed therein.

FUNDING

The authors gratefully acknowledge the financial support from the European Research Council through the AdG-340685-MicroMotility and from the Italian Ministry of University and Research (MIUR) through the grant Dipartimenti di Eccellenza 2018-2022 (Mathematics Area).

ACKNOWLEDGMENTS

The authors would like to thank Alessandro Lucantonio for fruitful discussions and valuable suggestions. This manuscript has been released as a pre-print at: www.biorxiv.org/content/10.1101/2020.07.06.188987v1 (Agostinelli et al., 2020a), and it includes content that appeared in DA's Ph.D. thesis (Agostinelli, 2020).

SUPPLEMENTARY MATERIAL

The Supplementary Material for this article can be found online at: <https://www.frontiersin.org/articles/10.3389/fpls.2021.608005/full#supplementary-material>

Data Sheet 1 | Five Supplementary sections: Growing morphoelastic rods, the statoliths avalanche dynamics, stability analyses, computational model, and experimental materials and methods.

REFERENCES

- Agostinelli, D. (2020). *Mathematical models for biological motility: from peristaltic crawling to plant nutations* (Ph.D. thesis). SISSA, Trieste, Italy.
- Agostinelli, D., DeSimone, A., and Noselli, G. (2020a). Nutations in plant shoots: endogenous and exogenous factors in the presence of mechanical deformations. *bioRxiv [Preprint]*. doi: 10.1101/2020.07.06.188987
- Agostinelli, D., Lucantonio, A., Noselli, G., and DeSimone, A. (2020b). Nutations in growing plant shoots: the role of elastic deformations due to gravity loading. *J. Mech. Phys. Solids* 136:103702. doi: 10.1016/j.jmps.2019.103702

Data Sheet 2 | Experimental Data. We provide 4 csv files (data_fig1A.csv, data_fig1B.csv, data_fig1C.csv, and data_video.csv) with the tip trajectories shown in this article (**Figures 1, 7** and **Video 1**), as reconstructed from the experiments (see **Supplementary Material**, section S5).

Video 1 | Experiment and data analysis. This video shows the tracking and reconstruction of a flower of the primary inflorescence in a 29-day-old sample of *Arabidopsis thaliana* (ecotype Col-0) grown under normal gravity conditions (1 g) and continuous light at the SAMBA laboratory of SISSA. The images were acquired by using two digital cameras, namely, two acA4024-29uc c mount cameras from Basler, both of which were equipped with an objective m0824-mpw2 from Computar. The points (black dots) were tracked on the stereo pair of images, which were calibrated to reconstruct the 3D position by exploiting the Computer Vision Toolbox in MATLAB R2019b. The colored lines, from blue to red for increasing time, are obtained by moving averaging over ten detected positions. The red dot indicates the base of the plant.

Video 2 | A growing shoot. Computational results from the full model (S3.1) for $\ell_0 = 6.8$ cm, $\ell_g = 7$ cm, $\alpha = 0.2$, $\beta = 0.8$, $\eta = 20$, $\tau_a = 2$ min, $\tau_m = \tau_r = \bar{\tau}_m = \bar{\tau}_r = 12$ min, $\tau_e = 24$ min, $\tau_g = 40$ h, $\tau_\ell = 6$ d, $r = 0.5$ mm, $\rho = 10^3$ Kg m⁻³, $E_0 = 10^7$ Pa, $E_1 = 200E_0$, and $\nu = 0.5$. We notice that the critical length for the stability of the corresponding reduced model (S3.5) is given by $\ell^* \approx 7.24$ cm for the chosen model parameters. Here black arrows denote the statoliths local orientations (**h**), while the other three are the directors (**d**₁, **d**₂ and **d**₃). In the beginning we observe only endogenous oscillations with gravitropic and proprioceptive responses. In the intermediate regime endogenous and exogenous oscillations are comparable and give rise to trochoid-like patterns. In the end, the second ones dominate the oscillatory movements.

Video 3 | A growing shoot. Same as in **Video 2** but for $\alpha = 0.01$. Differently from **Video 2**, intrinsic cues have little influence and the growing shoot tends to circular patterns passing by elliptic trajectories.

Video 4 | Limit cycles. Computational results from the reduced model (S3.5) but equipped with the statolith avalanche dynamics (6). Model parameters are $\ell = 6.59$ cm, $\alpha = 0$, $\beta = 0.8$, $\eta = 20$, $\tau_m = \tau_r = \bar{\tau}_m = \bar{\tau}_r = 12$ min, $\tau_a = 2$ min, $\tau_g = 20$ h, $r = 0.5$ mm, $\rho = 10^3$ Kg m⁻³, $E = 10^7$ Pa, and $\nu = 0.5$. Black arrows denote the statoliths local orientations (**h**), while the other three are the directors (**d**₁, **d**₂ and **d**₃). We initially perturb the model with an apical load $\epsilon \sin(\pi t/12)$ ($2\mathbf{e}_1 + \mathbf{e}_3$) where $\epsilon = 10^{-5}$ N for $t \in [0, 12]$ min, and $\{\mathbf{e}_1, \mathbf{e}_2, \mathbf{e}_3\}$ is a fixed orthonormal basis. Upon such a perturbation, the solution tends to pendular oscillations until an orthogonal apical load $\epsilon \sin[\pi(t - 1800)/12]$ ($\mathbf{e}_1 - 2\mathbf{e}_3$) is applied for $t \in [1800, 1812]$ min. Then the solution tends to the stable circular limit cycle by describing elliptic spirals.

Video 5 | Epitrochoid-like patterns. Same model as in **Video 4**, but for $\alpha = 0.3$, $\tau_e = 20$ min and $\ell = 6.565$ cm. In order to speed up the convergence to periodic oscillations, we introduced some perturbations as apical loads at different time intervals (not shown).

Video 6 | Hypotrochoid-like patterns. Same as in **Video 5** but with opposite angular velocity for the internal oscillator.

- Agostinelli, D., Noselli, G., and DeSimone, A. (in press). Nutations in growing plant shoots as a morphoelastic flutter instability. *Philos. Trans. R. Soc. A Math. Phys. Eng. Sci.*
- Antman, S. (2005). *Nonlinear Problems of Elasticity*. New York, NY: Springer-Verlag.
- Bastien, R., Douady, S., and Moulia, B. (2014). A unifying modeling of plant shoot gravitropism with an explicit account of the effects of growth. *Front. Plant Sci.* 5:136. doi: 10.3389/fpls.2014.00136
- Bastien, R., and Meroz, Y. (2016). The kinematics of plant nutation reveals a simple relation between curvature and the orientation of differential growth. *PLoS Comput. Biol.* 12:e1005238. doi: 10.1371/journal.pcbi.1005238

- Berg, A., and Peacock, K. (1992). Growth patterns in nutating and nonnutating sunflower (*Helianthus annuus*) hypocotyls. *Am. J. Bot.* 79, 77–85. doi: 10.1002/j.1537-2197.1992.tb12626.x
- Bigoni, D., Kirillov, O., Misseroni, D., Noselli, G., and Tommasini, M. (2018). Flutter and divergence instability in the Pflüger column: Experimental evidence of the Ziegler destabilization paradox. *J. Mech. Phys. Solids* 116, 99–116. doi: 10.1016/j.jmps.2018.03.024
- Bigoni, D., and Noselli, G. (2011). Experimental evidence of flutter and divergence instabilities induced by dry friction. *J. Mech. Phys. Solids* 59, 2208–2226. doi: 10.1016/j.jmps.2011.05.007
- Buda, A., Zawadzki, T., Krupa, M., Stolarz, M., and Okulski, W. (2003). Daily and infradian rhythms of circumnutation intensity in *Helianthus annuus*. *Physiol. Plant.* 119, 582–589. doi: 10.1046/j.1399-3054.2003.00198.x
- Chauvet, H., Mouliat, B., Legué, V., Forterre, Y., and Pouliquen, O. (2019). Revealing the hierarchy of processes and time-scales that control the tropic response of shoots to gravi-stimulations. *J. Exp. Bot.* 70, 1955–1967. doi: 10.1093/jxb/erz027
- Chelakkot, R., and Mahadevan, L. (2017). On the growth and form of shoots. *J. R. Soc. Interface* 14:20170001. doi: 10.1098/rsif.2017.0001
- Correll, M., and Kiss, J. (2002). Interactions between gravitropism and phototropism in plants. *J. Plant Growth Regul.* 21, 89–101. doi: 10.1007/s003440010056
- Darwin, C. (1880). *The Power of Movement in Plants*. London: John Murray.
- Erickson, R., and Sax, K. (1956). Elemental growth rate of the primary root of zeamays. *Proc. Am. Philos. Soc.* 100, 487–498.
- Forterre, Y., Skotheim, J., Dumais, J., and Mahadevan, L. (2005). How the venus flytrap snaps. *Nature* 433, 421–425. doi: 10.1038/nature03185
- Goriely, A. (2017). *The Mathematics and Mechanics of Biological Growth*, Vol. 45. New York, NY: Springer.
- Gradmann, H. (1922). Die Fünfphasenbewegung der Ranken. *Jahrbücher Wissenschaft. Bot.* 61, 169–204.
- Greenhill, A. (1881). Determination of the greatest height consistent with stability that a vertical pole or mast can be made, and of the greatest height to which a tree of given proportions can grow. *Proc. Camb. Philos. Soc.* 4, 65–73.
- Hall, H., and Ellis, B. (2012). Developmentally equivalent tissue sampling based on growth kinematic profiling of arabidopsis inflorescence stems. *New Phytol.* 194, 287–296. doi: 10.1111/j.1469-8137.2012.04060.x
- Hofhuis, H., Moulton, D., Lessinnes, T., Routier-Kierzkowska, A.-L., Bomphrey, R., Mosca, G., et al. (2016). Morphomechanical innovation drives explosive seed dispersal. *Cell* 166, 222–233. doi: 10.1016/j.cell.2016.05.002
- Israelsson, D., and Johnsson, A. (1967). A theory for circumnutations in *Helianthus annuus*. *Physiol. Plant.* 20, 957–976. doi: 10.1111/j.1399-3054.1967.tb08383.x
- Johnsson, A., Jansen, C., Engelmann, W., and Schuster, J. (1999). Circumnutations without gravity: a two-oscillator model. *J. Gravit. Physiol.* 6, 9–12.
- Johnsson, A., Solheim, B., and Iversen, T.-H. (2009). Gravity amplifies and microgravity decreases circumnutations in *Arabidopsis thaliana* stems: results from a space experiment. *New Phytol.* 182, 621–629. doi: 10.1111/j.1469-8137.2009.02777.x
- Kobayashi, A., Kim, H.-J., Tomita, Y., Miyazawa, Y., Fujii, N., Yano, S., et al. (2019). Circumnutational movement in rice coleoptiles involves the gravitropic response: analysis of an agravitropic mutant and space-grown seedlings. *Physiol. Plant.* 165, 464–475. doi: 10.1111/ppl.12824
- Levernier, N., Pouliquen, O., and Forterre, Y. (2021). An integrative model of plant gravitropism linking statoliths position and auxin transport. *bioRxiv [Preprint]*. doi: 10.1101/2021.01.01.425032
- Logg, A., Mardal, K.-A., and Wells, G. (2012). *Automated Solution of Differential Equations by the Finite Element Method: The FEniCS Book*, Vol. 84. Berlin; Heidelberg: Springer Berlin Heidelberg. doi: 10.1007/978-3-642-23099-8
- Maksymowych, R., Maksymowych, A., and Orkwiszewski, J. (1985). Stem elongation of xanthium plants presented in terms of relative elemental rates. *Am. J. Bot.* 72, 1114–1119. doi: 10.1002/j.1537-2197.1985.tb08359.x
- Mazzolai, B. (2017). “Plant-inspired growing robots,” in *Soft Robotics: Trends, Applications and Challenges*, eds C. Laschi, J. Rossiter, F. Iida, M. Cianchetti, and L. Margheri (Springer Nature), 57–63. Available online at: <https://link.springer.com/book/10.1007/978-3-319-46460-2>
- Meroz, Y., Bastien, R., and Mahadevan, L. (2019). Spatio-temporal integration in plant tropisms. *J. R. Soc. Interface* 16:20190038. doi: 10.1098/rsif.2019.0038
- Moulton, D., Oliveri, H., and Goriely, A. (2020). Multiscale integration of environmental stimuli in plant tropism produces complex behaviors. *Proc. Natl. Acad. Sci. U.S.A.* 117, 32226–32237. doi: 10.1101/2020.07.30.228973
- Mugnai, S., Azzarello, E., Masi, E., Pandolfi, C., and Mancuso, S. (2015). “Nutation in plants,” in *Rhythms in Plants*, eds S. Mancuso and S. Shabala (Springer), 19–34. Available online at: <https://www.springer.com/gp/book/9783319205168>
- Mullen, J., Ishikawa, H., and Evans, M. (1998). Analysis of changes in relative elemental growth rate patterns in the elongation zone of arabidopsis roots upon gravistimulation. *Planta* 206, 598–603. doi: 10.1007/s004250050437
- Nakamura, M., Nishimura, T., and Morita, M. (2019). Gravity sensing and signal conversion in plant gravitropism. *J. Exp. Bot.* 70, 3495–3506. doi: 10.1093/jxb/erz158
- Niinuma, K., Someya, N., Kimura, M., Yamaguchi, I., and Hamamoto, H. (2005). Circadian rhythm of circumnutation in inflorescence stems of *Arabidopsis*. *Plant Cell Physiol.* 46, 1423–1427. doi: 10.1093/pcp/pci127
- Okamoto, K., Ueda, H., Shimada, T., Tamura, K., Kato, T., Tasaka, M., et al. (2015). Regulation of organ straightening and plant posture by an actin-myosin XI cytoskeleton. *Nat. Plants* 1:15031. doi: 10.1038/nplants.2015.31
- Paul-Victor, C., and Rowe, N. (2011). Effect of mechanical perturbation on the biomechanics, primary growth and secondary tissue development of inflorescence stems of arabidopsis thaliana. *Ann. Bot.* 107, 209–218. doi: 10.1093/aob/mcq227
- Phyo, P., Wang, T., Kiemle, S., O'Neill, H., Pingali, S., Hong, M., et al. (2017). Gradients in wall mechanics and polysaccharides along growing inflorescence stems. *Plant Physiol.* 175, 1593–1607. doi: 10.1104/pp.17.01270
- Porat, A., Tedone, F., Palladino, M., Marcati, P., and Meroz, Y. (2020). A general 3d model for growth dynamics of sensory-growth systems: from plants to robotics. *Front. Robot. AI* 7:89. doi: 10.3389/frobt.2020.00089
- Schuster, J., and Engelmann, W. (1997). Circumnutations of *Arabidopsis thaliana* seedlings. *Biol. Rhythm Res.* 28, 422–440. doi: 10.1076/brhm.28.4.422.13117
- Shabala, S. (2003). “Physiological implications of ultradian oscillations in plant roots,” in *Roots: The Dynamic Interface Between Plants and the Earth*, ed J. Abe (Dordrecht: Springer), 217–226.
- Shabala, S., and Newman, I. (1997). Proton and calcium flux oscillations in the elongation region correlate with root nutation. *Physiol. Plant.* 100, 917–926. doi: 10.1111/j.1399-3054.1997.tb00018.x
- Stolarz, M. (2009). Circumnutation as a visible plant action and reaction: physiological, cellular and molecular basis for circumnutations. *Plant Signal. Behav.* 4, 380–387. doi: 10.4161/psb.4.5.8293
- Su, S.-H., Gibbs, N., Jancewicz, A., and Masson, P. (2017). Molecular mechanisms of root gravitropism. *Curr. Biol.* 27, R964–R972. doi: 10.1016/j.cub.2017.07.015
- Tsugawa, S., Kanda, N., Nakamura, M., Goh, T., Ohtani, M., and Demura, T. (2020). Spatio-temporal kinematic analysis of shoot gravitropism in *Arabidopsis thaliana*. *Plant Biotechnol.* 37, 443–450. doi: 10.5511/plantbiotechnology.20.0708a
- van der Weele, C., Jiang, H., Palaniappan, K., Ivanov, V., Palaniappan, K., and Baskin, T. (2003). A new algorithm for computational image analysis of deformable motion at high spatial and temporal resolution applied to root growth. roughly uniform elongation in the meristem and also, after an abrupt acceleration, in the elongation zone. *Plant Physiol.* 132, 1138–1148. doi: 10.1104/pp.103.021345

Conflict of Interest: The authors declare that the research was conducted in the absence of any commercial or financial relationships that could be construed as a potential conflict of interest.

Copyright © 2021 Agostinelli, DeSimone and Noselli. This is an open-access article distributed under the terms of the Creative Commons Attribution License (CC BY). The use, distribution or reproduction in other forums is permitted, provided the original author(s) and the copyright owner(s) are credited and that the original publication in this journal is cited, in accordance with accepted academic practice. No use, distribution or reproduction is permitted which does not comply with these terms.